ON THE EFFECT OF AN OVERLOAD TO FATIGUE CRACK GROWTH

Yang Bingxian (杨秉宪)
Beijing Institute of Aeronautics and Astronautics, China

H.Miyamoto, M.Kikuchi, K.Machida, and K.Kawashima
Department of Mechanical Engineering, Faculty of Science and Technology,
Science University of Tokyo, Noda, Chiba(278), Japan

I. INTRODUCTION

In this paper, the fatigue crack growth behavior resulting from a single overload is investigated for 7075—T6 aluminium alloy. In order to clarify the mechanisms of overload effect on fatigue crack growth, the crack closure and opening processes and their levels are detected by the strain gage on the back surface of specimens, and the fracture surface morphologies are examined by the microfractography.

II. EXPERIMENTAL PROCEDURE

The material used is 7075—T6 alluminium alloy. The chemical compositions and mechanical properties of the material are shown in tables 1 and 2, respectively. Compact tension specimen, 50.8 mm width and 10 mm thick, are used.

Retardation tests are performed by a 490 KN MTS electohydraulic closed loop testing machine at a cyclic frequency of 10Hz. Single peak overloads are introduced with a frequency of 0.1Hz.

In order to identify overload interaction induced variations in fatigue crack growth rate, all tests are performed under constant ΔK_1 conditions. The constant ΔK_1 levels are maintained by load spectrum as is schematically represented in Fig. 1. In a case of large scale yielding, the J integral range, ΔJ, must be used as a parameter for the fatigue

crack growth. ΔJ is calculated from the load versus displacement record by the Clarke's formulation:

$$\Delta J = \frac{2A(1+\alpha)}{Bb(1+\alpha^2)} \tag{1}$$

$$\alpha = \sqrt{(2a/b)^2 + 2(2a/b) + 2} - (2a/b + 1),\ b = W-a \tag{2}$$

where A is an area under the load-displacement record, B is the specimen thickness, and W is the specimen width.

The retardation behavior observed is correlated with the crack closure detected by the strain gage on the back surface of specimens as shown in Fig.2. After fatigue tests, fracture surfaces of specimens are investigated by using a scanning electron microscope.

III. RESULTS AND DISCUSSIONS

The typical $(a-a_0)$ vs. $(N-N_0)$ and da/dN vs. $(a-a_0)$ curves during retardation are plotted in Fig. 3 and 4, in which r means the ratio of ΔK_2 to ΔK_1 shown in Fig. 1. All samples show similar pattern of the delayed retardation, that is, the fatigue crack growth rate becomes the minimum after the crack has propagated a small distance from the overloading.

Fig. 5 shows the typical variations of back surface strain, ε_b. Fig. 6 shows the crack tip opening levels, plotted from Fig. 5, where ε_e is the elastic strain, and ε_0 is the maximum range of ε_b. The K value, given by the zero point of abscissa, is the crack opening level K_{op}. It is shown that the crack opening level is once lowered by the application of the overload, and rises up beyond the level before overload. It reaches to the maximum level followed by a gradual lowering to the stabilized level. This phenomenon may be related to the delayed retardation behaviors by the overload.

Fig. 7 and 8 show the typical scanning electron fractographs of fatigue crack surfaces. They are the results by high level overloads. Fig. 7(a) and 8(a) show the striation spacing S_t, and crack growth rate da/dN measured on the surfaces of a specimen vs. crack growth increments $(a-a_0)$. Fig. 7(b) and 8(b) show the shapes of crack fronts following an overload, plotted by the micrographic observations. Fig. 7(c) and 8(c) show the photographs of fracture surfaces, in which dark markings mean the ductile fracture surfaces by the overload.

For high overload levels, the fracture surface micromorphologies corresponding to the retardation phase in the central region of the specimen are different from those in the vicinity of the specimen surfaces. In the central region, equiaxed dimples are observed on ductile fracture surfaces as shown in Photo. 6 and 7 in Fig.9. They mean coalesced voids. Then the crack propagates by quasi-cleavage followed by the formation of striation as shown in Photo.4, 1, and 2. Near specimen surfaces, the overload produces a slip and develops into striation as shown in Photo.8, 5, and 3. These observations are consistent with the references [1,2]. The shapes and the orientations of striations are not regular due to the effects of the inclusions and second phase particles in the specimen as shown in Photo. A and B.

IV. CONCLUSIONS

The observation of the processes developing at the fatigue crack tip for 7075-T6, leads us to introduce some explanations on the mechanisms of retardation after a single overload.

(1) For high level overloads, a dark marking, representing the ductile fracture by the overload, is observed . The fracture surface micromorphologies corresponding to the retardation phases at the central region of the specimen are different from those of near surface.

(2) The mechanisms of an overload effect on fatigue crack growth are the variables of plasticity induced by crack closure and the change in effective stress intensity factor range, ΔK_{eff}. The residual stresses at the crack tip assaociated with the crack tip blunting seems to be the most reasonable physical explanation for these phenomena.

REFERENCES

[1] Yang Bing-Xian, A Crack Growth Model under Spectrum Loading. Pro. of 13rd Congress of the International Council of the Aeronautical Sciences. 1982 (Seattle).

[2] Bathias,C, and Vancon, M., Mechanisms of overload Effect on Fatigue Crack Propagation in Aluminium Alloys. Engng.Fracture Mech. 10,409-424 (1978).

Table 1 Chemical compositions (wt%).

Si	Fe	Cu	Ti	Mn	Cr	Zn	Mg
0.15	0.21	1.50	0.07	0.00	0.21	5.50	2.60

Table 2 Mechanical properties.

σ_{YS} (MPa)	σ_B (MPa)	E (GPa)	T.E. (%)
375.3	463.5	71.8	14

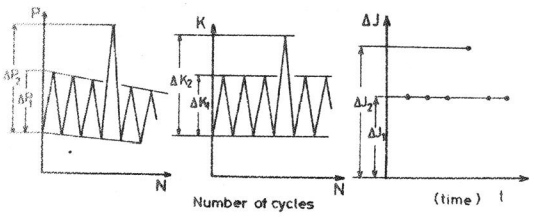

Fig.1 Schematic representation of test spectrum.

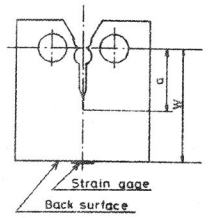

Fig.2 Position of strain gage on the CT specimen.

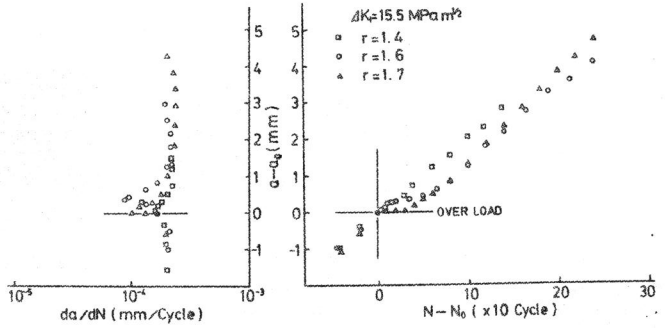

Fig.3 Experimental results of crack growth for lower overload levels.

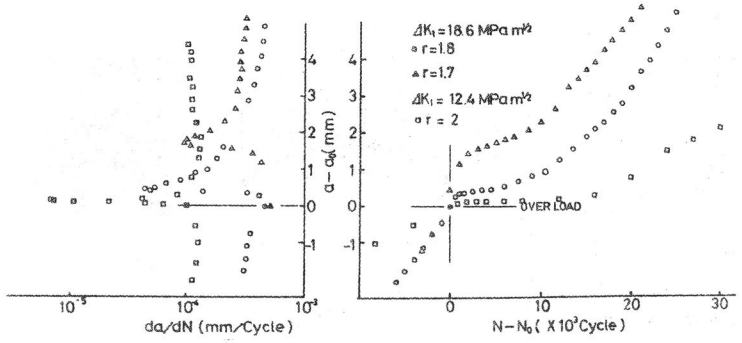

Fig.4 Experimental results of crack growth for high overload levels.

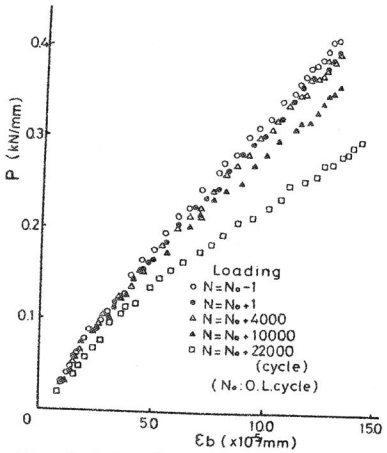

Fig.5 Relation between load P and back surface strain ε_b.

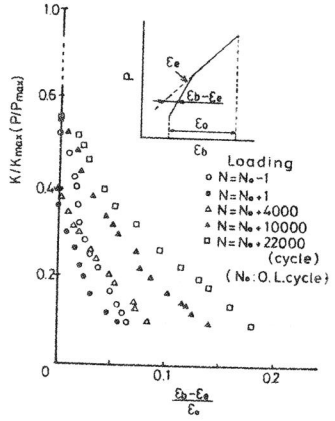

Fig.6 Relation between K/K_{max} and $(\varepsilon_b-\varepsilon_e)/\varepsilon_0$.

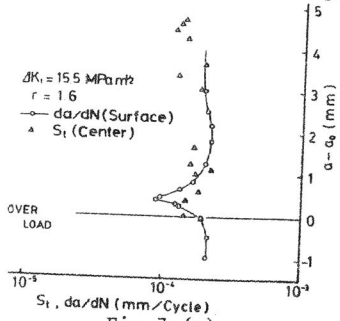

Fig.7-(a)

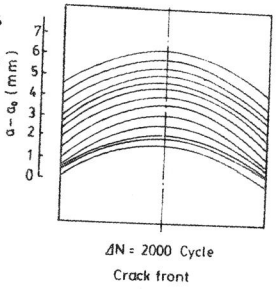

Fig.7-(b)

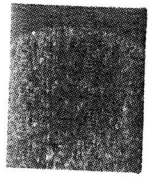

Fig.7-(c)

Fig.7 Typical fractograph of fracture surface for lower overload level.

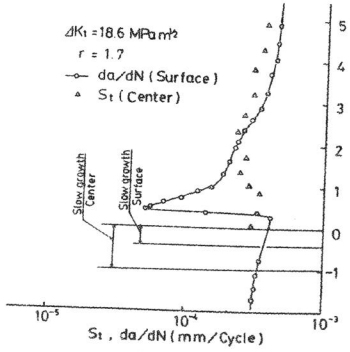

Fig.8-(a)

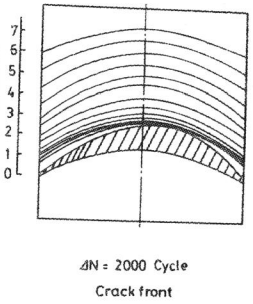

Fig.8-(b)

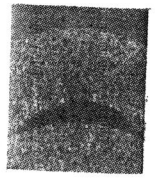

Fig.8-(c)

Fig.8 Typical fractograph of fracture surface for high overload level.

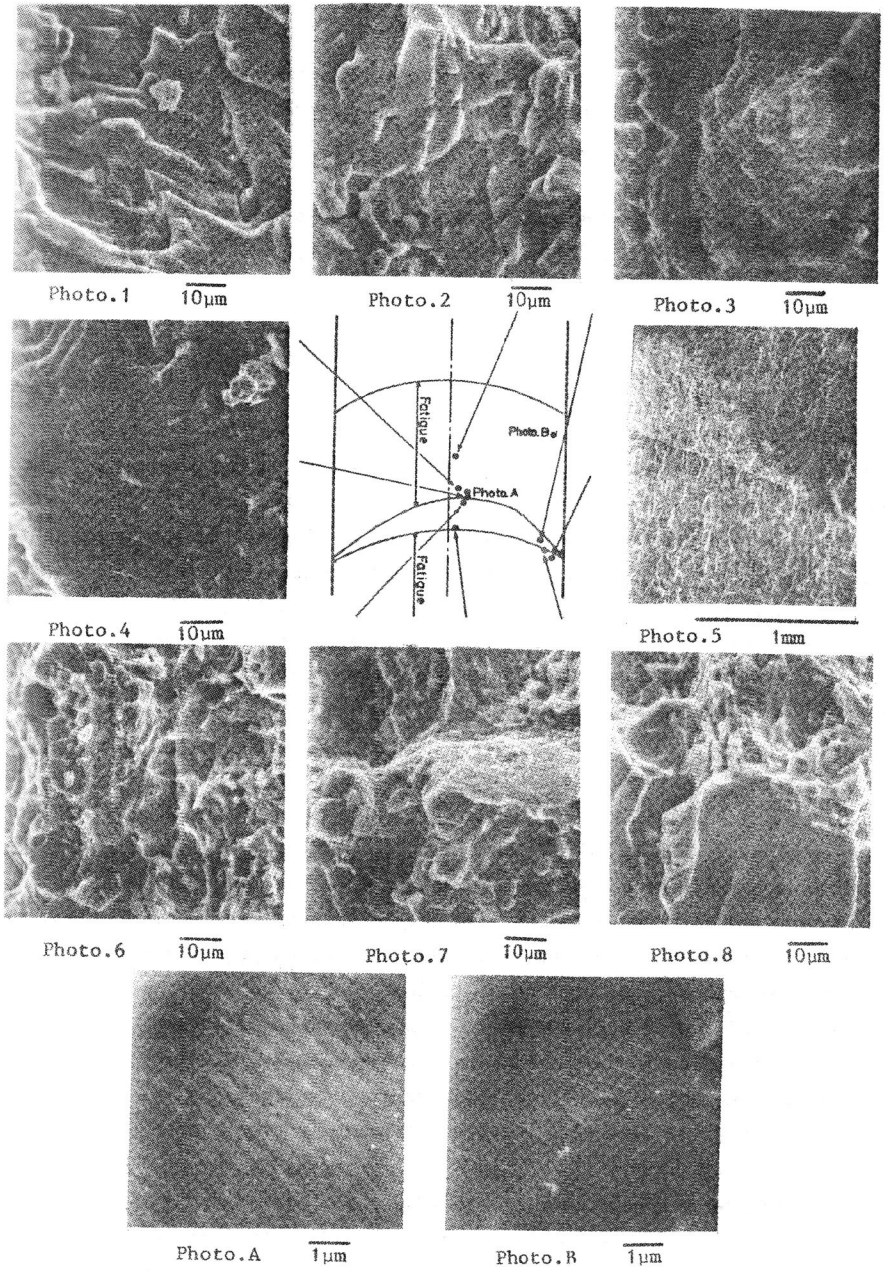

Fig.9 Typical fracture surface micromorphology for high overload level.